STM JOURNALS

Nano Trends:
A Journal of Nanotechnology and Its Applications

ISSN: 0973-418X
Volume 27, Issue 3, 2025
September–December
DOI (Journal): 10.37591/NTs

https://journals.stmjournals.com/nts

Review NTs

Preparation and Characterization of High-Performance ZnO/PVB Nanocomposite Films for UV-Shielding and Optoelectronics

Rajeshwar Reddy A.[1,*], J. Satheesh Goud[2], N. Narsimulu[3]

Abstract

Zinc oxide nanoparticles can be incorporated into polymer matrices to create materials for various high-performance engineering applications. In this study, zinc oxide nanoparticles were reinforced at different loadings (0.5, 1.0, 0.5, 1.0, 1.5, and 2.0 wt.%) in polyvinyl butyral matrix to synthesize nanocomposite films using the solution casting method. The impact of zinc oxide nanofiller on the morphology and ultraviolet-shielding performance of polyvinyl butyral nanocomposite films was evaluated using various characterization techniques. The zinc oxide nanoparticles are well dispersed in the polyvinyl butyral polymer matrix, as shown by the X-ray diffraction patterns and scanning electron microscopy micrographs. The energy dispersive X-ray analysis confirms the quantitative presence of zinc oxide in the composite films. The absorption peaks in the Fourier-transform infrared spectroscopy spectra of the nanocomposites shift to higher or lower wavenumbers compared to those observed in pure polyvinyl butyral. These shifts are associated with the interaction between zinc oxide and the molecular chains of polyvinyl butyral. Ultraviolet-visible absorption spectroscopy assessed optical characteristics, film transparency, and ultraviolet-shielding performance. Specifically, the composite films containing 2.0 wt.% of zinc oxide in polyvinyl butyral exhibit a 21.4% enhancement in ultraviolet-shielding compared to pure polyvinyl butyral while maintaining acceptable transparency. Therefore, these nanocomposite films can be used in various engineering applications, including ultraviolet-shielding and optoelectronics devices.

Keywords: Zinc oxide (ZnO)/polyvinyl butyral (PVB) nanocomposite films, X-ray diffraction (XRD), scanning electron microscopy (SEM), Fourier-transform infrared spectroscopy (FTIR), UV-visible spectroscopy, UV-shielding

***Author for Correspondence**
Rajeshwar Reddy A.
E-mail: rajeshwarreddy82@gmail.com

[1]Lecturer, Department of Physics, MJPTBCWR Junior College for Girls (COE), Hyderabad, Telangana, India
[2]Degree Lecturer in Physics & O.S.D. (Degree Colleges), Telangana Tribal Welfare Residential Educational Institutions Society, Hyderabad, Telangana, India
[3]Associate Professor, Department of Physics, University College of Engineering, Osmania University, Hyderabad, Telangana, India

Received Date: May 21, 2025
Accepted Date: June 05, 2025
Published Date: July 01, 2025

Citation: Rajeshwar Reddy A., J. Satheesh Goud, N. Narsimulu. Preparation and Characterization of High-Performance ZnO/PVB Nanocomposite Films for UV-Shielding and Optoelectronics. Nano Trends: A Journal of Nanotechnology and Its Applications. 2025; 27(3): 35–53p.

INTRODUCTION

Utilizing materials and devices at the nanoscale and employing various techniques is the key aspect of modern nanotechnology (MNT), which is already being applied across many scientific disciplines [1]. Nanoparticles (NPs) are characterized by their unique properties and extraordinarily high surface area-to-volume ratio. Due to the excellent characteristics of zinc oxide (ZnO) NPs, they have gained popularity in recent years for developing innovative, cutting-edge applications [2]. The similar dimensions of ZnO NPs and their significant reactivity in the free state are two factors that contribute to their distinctive properties and utility [3]. NPs can be produced using various synthesis

methods, which impart essential features, such as ultraviolet (UV) shielding and optoelectronic capabilities. As the size decreases, particles become highly reactive and exhibit notable physical and chemical properties because their constituent atoms are near the surface.

Many types of NPs have been reported in research literature. Examples include metal NPs, metal oxide NPs, and polymer NPs [4]. Among these, metal oxide NPs are the most versatile materials due to their wide range of properties and functions. Among the various metal oxide NPs, ZnO NPs are readily available and preferred for multiple applications. Its wide bandgap (3.37 eV), excellent bond strength, and large exciton binding energy (60 MeV) at ambient temperature make it an appealing material for short-wavelength optoelectronic applications [5]. It is also used in developing solid-state optoelectronics, ranging from blue to UV and laser technology [6].

ZnO NPs are safe and absorb significant amounts of UV light, making them an excellent choice for modern technology [7]. The structure of these NPs is also stiff and rigid, rendering them useful in the polymer industry. ZnO/polymer composites possess outstanding properties that enhance their utility in various aspects of nanoscience. ZnO exists in different forms, like NPs, nanowires, nanofibers, and other nanostructures, utilized across multiple fields. The performance of ZnO NPs differs significantly from that of bulk materials with equivalent properties. The polymer industry is currently focused on synthesizing low-cost polymer composites with favorable properties by dispersing small quantities of ZnO NPs [8].

EXPERIMENTAL DETAILS

Materials Used in This Work and Their Technical Data (Table 1).

Table 1. Details of materials used in the preparation of PVB–ZnO composites.

S.N.	Material	Physical Parameters	Material Form/Color	Supplier	Place
1.	Polyvinyl butyral (PVB)	Molar mass: 300.395 g/mol, melting point: 90–120°C	Powder/white	Rolex Chemical Industries	Bengaluru
2.	ZnO	Average particle size: 10–40 nm, purity > 99%, surface area: 100–120 m^2/g	Nano powder/ white	Ad-Nano Technologies	Shimoga
3.	Chloroform	Molecular weight: 119.38 g/mol, minimum assay (GC): 99.5%	Liquid	Molychem Laboratories	Mumbai
4.	Petri dishes	High-quality polytetrafluoroethylene (PTFE) diameter: 60 mm	Solid white dishes	Canfort Laboratory	USA

Synthesis of Pure PVB Film

A simple method known as solution casting was used to prepare pure PVB films. Three grams of polyvinyl butyral were dissolved in 60 ml of chloroform in a 100-ml beaker and stirred at 600 rpm with a magnetic stirrer at ambient temperature for 48 hours. After this process, a clear, homogeneous, viscous polymer solution was produced. The prepared solution was poured into Teflon petri dishes [9]. These dishes were left to dry at ambient temperature and allowed to dry slowly over 30 days, resulting in ~0.33-mm-thick PVB films being formed [10]. The films were peeled off from the dishes and cut into the required dimensions for further characterization [11]. The schematic diagram (step-by-step process) for the fabrication of PVB films is depicted in Figures 1 and 2.

Fabrication of ZnO/PVB Nanocomposite Films

As shown in Figure 3(a), the weight of PVB was set at 3.0 g for all concentrations to synthesize ZnO/PVB nanocomposite films. We prepared the PVB aqueous solution by dissolving 3.0 g of PVB in 30 ml of chloroform [12, 13]. Next, 0.5 wt.% of nano-sized ZnO was dissolved in 30 ml of chloroform and vigorously stirred for 2 hours. To achieve a homogeneous dispersion of ZnO in the polymer matrix, the obtained solutions were gradually mixed and stirred for 48 hours [14]. Following this process, the viscous gel was poured into Teflon petri dishes and kept at ambient temperature for 30 days to prepare

bubble-free nanocomposite films, as shown in Figure 3(b). The film was then peeled off from the petri dish, resulting in a ZnO/PVB nanocomposite film. The same procedure was used to synthesize 1.0, 1.5, and 2.0 wt.% ZnO NPs dispersed PVB nanocomposite films.

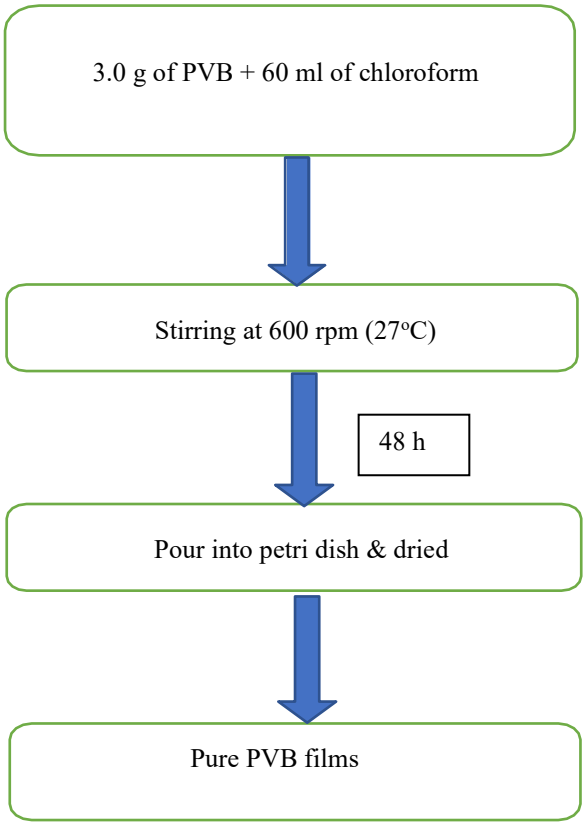

Figure 1. Schematic procedure for the synthesis of PVB films.

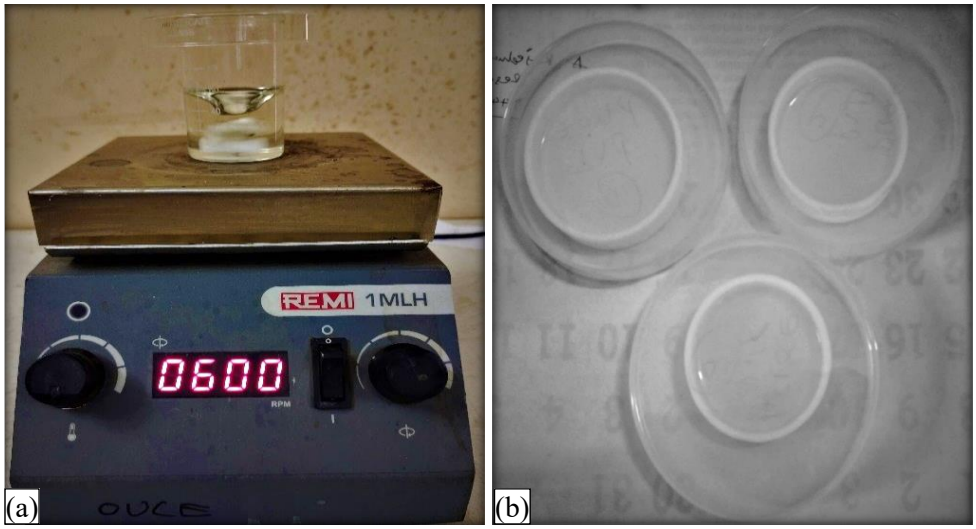

Figure 2. (a) stirring machine, (b) pure PVB films.

RESULTS AND DISCUSSION

X-Ray Diffraction (XRD) Analysis

The XRD patterns of ZnO NPs (Ad-Nano) and pure PVB are shown in Figure 4(a & b). A broad intensity peak was found at a scattering angle of $19° < 2\theta < 20°$ with an interplanar spacing (d) value of 0.45 nm for pure PVB. This indicates that the amorphous structure of PVB is mainly due to strong

intermolecular hydrogen bonding between monomer units [15]. As shown in Figure 5, the changes in the width of crystalline peaks observed after reinforcing ZnO NPs in the range of 2θ = 19°–22° reflect the changes in the crystalline phase of the PVB matrix. The intensity of the PVB crystalline peaks decreases up to a nanofiller concentration of 0.5 wt.%.

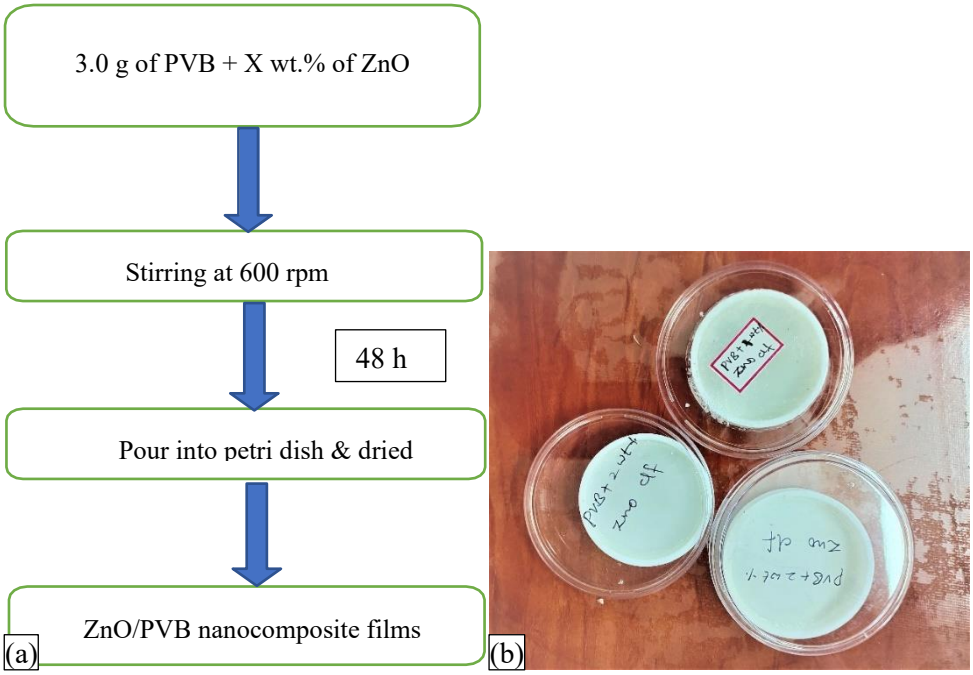

Figure 3. (a) Procedure for synthesis of ZnO/PVB nanocomposite films, (b) ZnO/PVB nanocomposite films.

Furthermore, beyond this concentration, the PVB peaks shift to a higher angle while maintaining the same intensity, resulting in a reduced crystalline phase of the composite films [15]. The dispersion of ZnO NPs within the PVB polymer accounts for the changes in the intensity of crystalline peaks. The hydrogen bonding between the OH groups of PVB and the ZnO NPs leads to an increase in the intermolecular distances among PVB chains [16, 17].

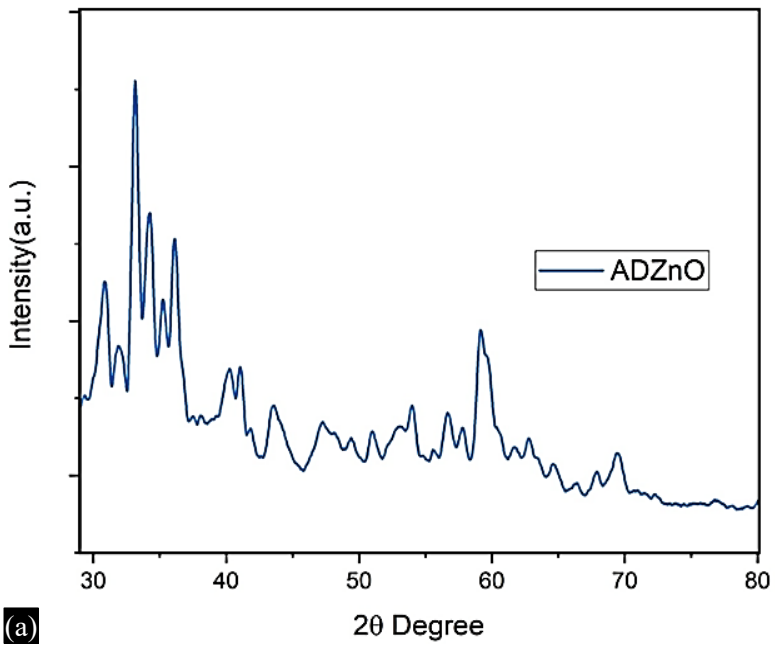

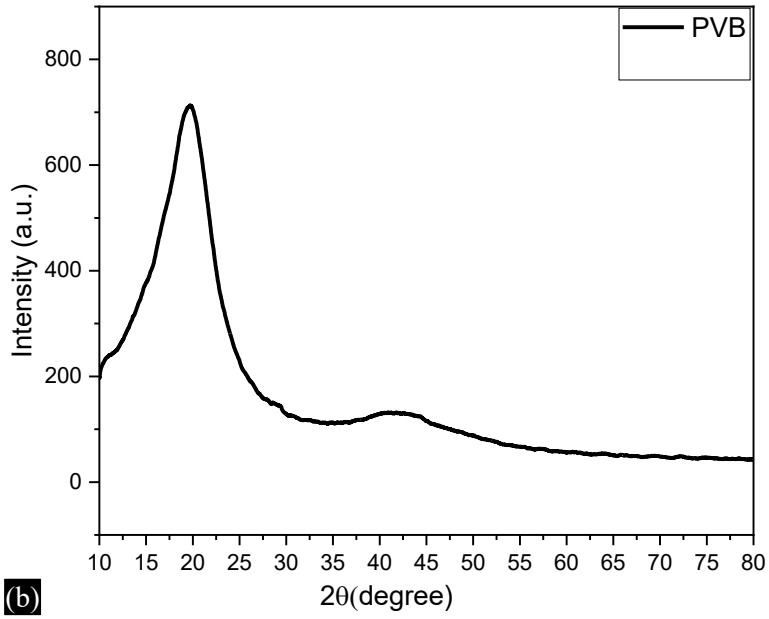

Figure 4. XRD fingerprints of (a) ZnO NPs and (b) pure PVB film.

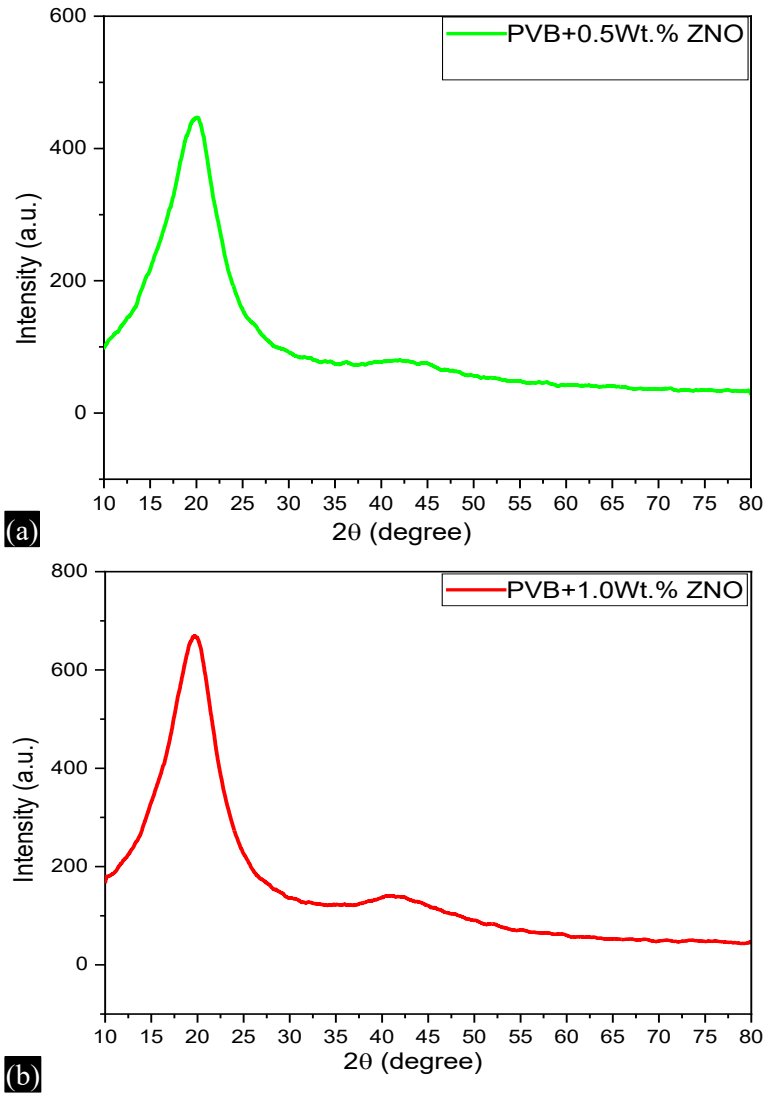

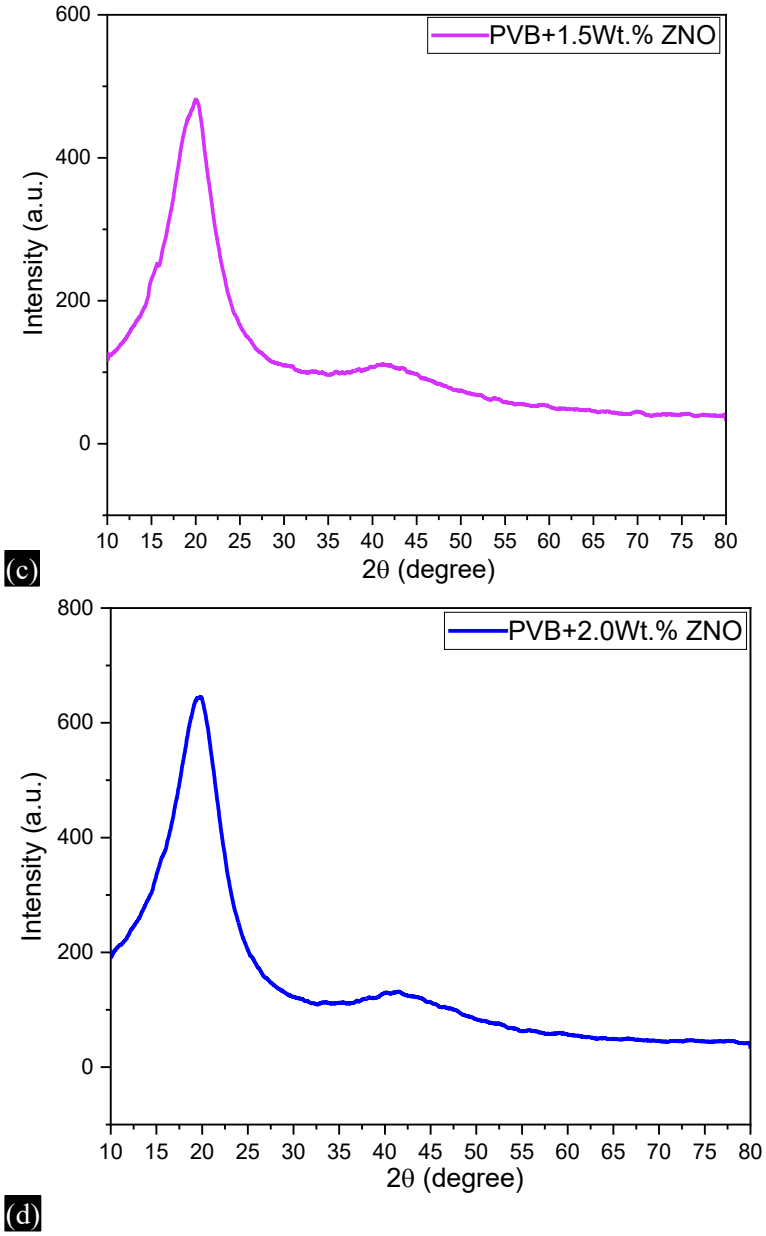

Figure 5. XRD fingerprints of ZnO/PVB nanocomposite films. (a) XRD pattern of PVB + 0.5 wt % ZnO, (b) XRD pattern of PVB + 1.0 wt % ZnO, (c) PVB + 1.5 wt % ZnO, (d) PVB + 2.0 wt % ZnO.

The average particle size (D) of composite films was determined to be approximately 49.0 nm by the Debye formula. The XRD studies of the samples reveal that PVB and nanocomposites with ZnO nanofiller exhibited reduced crystallinity. By comparing the XRD patterns of PVB and nanocomposites, it has been demonstrated that ZnO successfully maintained its structure after being dispersed in PVB during the synthesis process. Additionally, the peaks of ZnO/PVB indicate that ZnO NPs are uniformly distributed within the polymer.

Scanning Electron Microscopy (SEM)

The morphology of PVB and nanocomposite films was characterized using SEM. Figure 6(a–e) shows the SEM images of PVB and ZnO/PVB nanocomposites with 0.5, 1.0, 1.5, and 2.0 wt.% of ZnO. In nanocomposite films, the particle distribution is uniform throughout the matrix. It is also observed that many aggregate particles and pores have been reduced due to the uniform distribution of ZnO particles. In nanocomposites, PVB molecules are interlinked with ZnO particles, responsible for their

electrical conductivity [18]. Figure 6 indicates the morphology of the composites, revealing a typical nanocluster structure made of many nanospheres. The smooth surface of PVB was lost after adding NPs, while the film's surface began to show particle shapes with increasing nanofiller content [19]. All the ZnO/PVB nanocomposites exhibited rough surfaces, which differed considerably from the smooth surface of pure PVB, demonstrating that ZnO had been effectively dispersed within the PVB polymer. The nanoscale size of the composites is favorable for their application as a functional filler that integrates the advantages of ZnO [20].

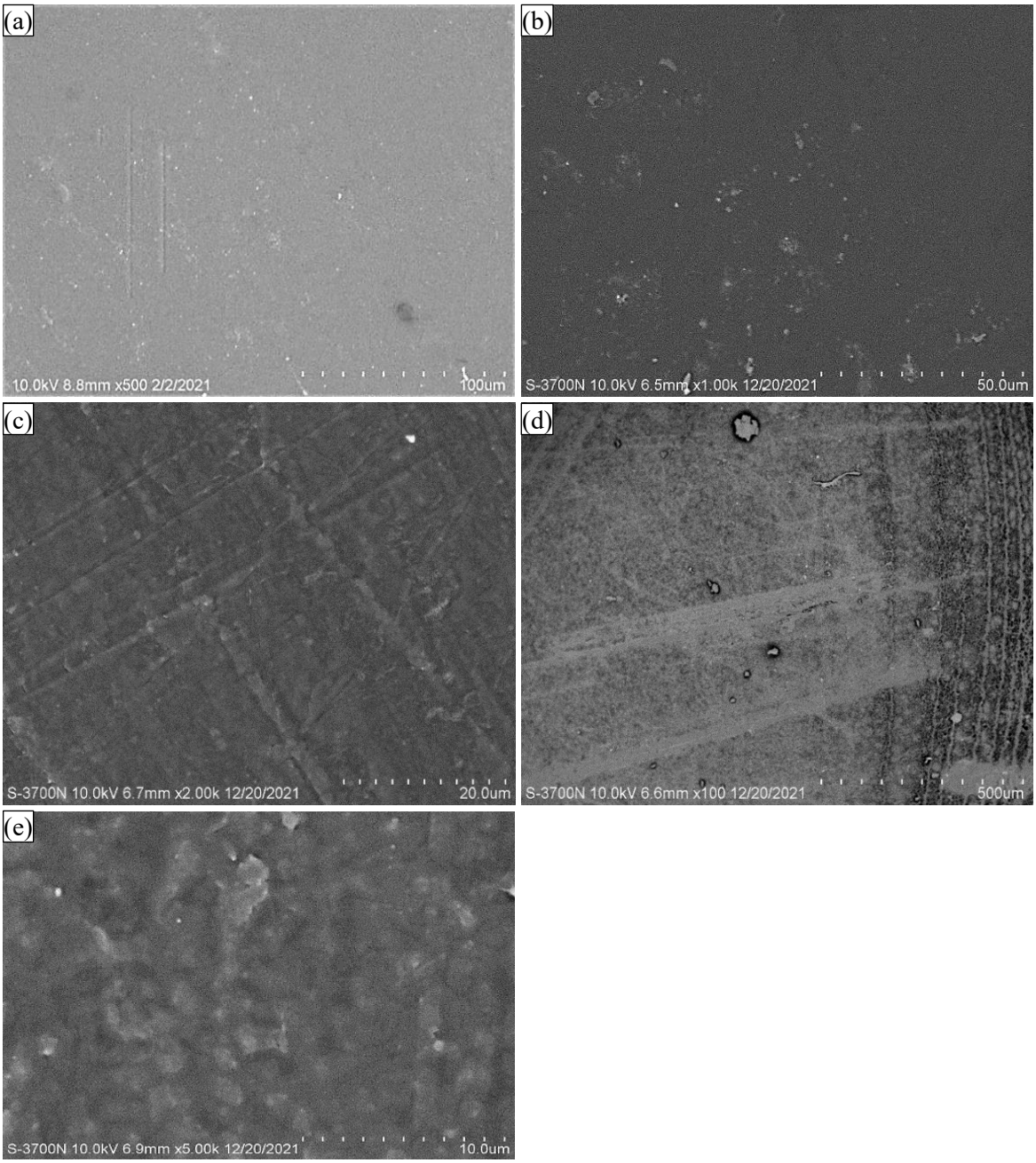

Figure 6. SEM micrographs of (a) pure PVB, (b) 0.5 wt.%, (c) 1.0 wt.%, (d) 1.5 wt.%, and (e) 2.0 wt. % of ZnO/PVB composite films.

Energy Dispersive Spectroscopy (EDS) Analysis

The appearance and surface morphology of nanocomposites were determined using standard SEM [21], while the chemical composition of the samples was evaluated using EDS analysis [19]. Figure

7(a) displays the results of the EDS investigation of the pure PVB film. The PVB film is stoichiometric and has a typical composition according to the EDS spectrum. In the EDS of the pure PVB, the characteristic X-ray peaks of the carbon atoms (66.82%; at. 72.84%) and oxygen (33.18%; at. 27.16%) are noticeable [22].

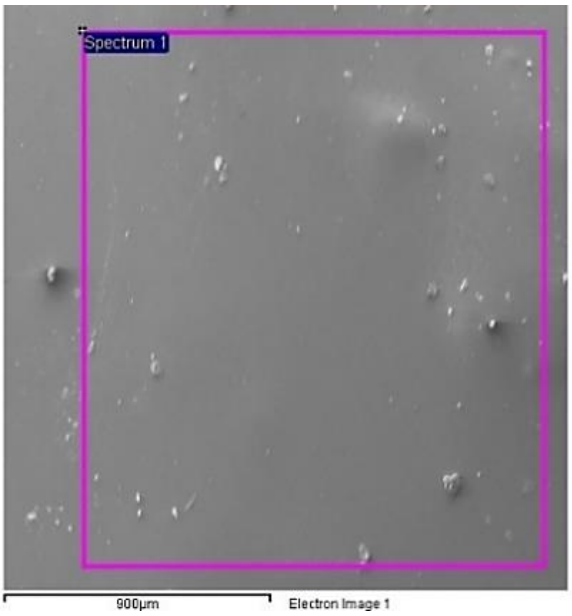

Element	Weight%	Atomic%
Carbon	66.81	72.83
Oxygen	33.17	27.15
Total	99.98	99.98

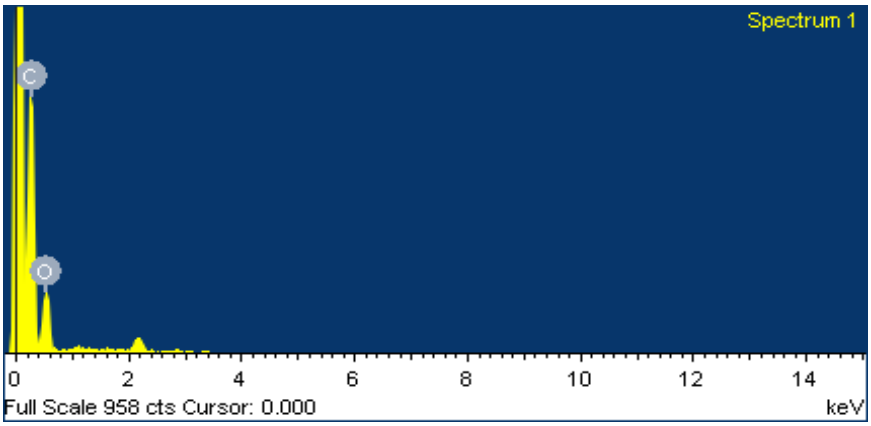

Figure 7. (a) EDS spectrum of pure PVB and elemental analysis.

Figure 7(b & c) shows that the synthesized nanocomposites were analyzed using a basic elemental mapping technique. In Figure 7(b & c), we observed that the identified atoms are carbon, oxygen, and zinc, by EDS analysis, appear as expected, and verified the produced nanocomposites. Alternatively, the results demonstrated uniform element distribution, noted purity, and no interfering elements were reported [20].

FTIR Analysis

The FTIR spectrum of PVB and ZnO/PVB nanocomposites is illustrated in Figure 8. The wavenumber range for this spectrum extends from 4000 to 500 cm^{-1}. The corresponding assignments are listed in Table 2. The O–H stretching vibration of the PVB functional groups is represented by the broad peak observed at 3434 cm^{-1}. The H–O–H vibration associated with the crystallization of water molecules can be identified by its peaks at 2360 cm^{-1}. The peaks observed at 1634 cm^{-1} and 1056 cm^{-1} are linked to the C=O stretching of an acetyl group and the C–C stretching in the butyral ring, respectively [21]. The presence of ZnO is confirmed by the small peaks identified between 515 and 560 cm^{-1}. Additionally, some peaks in the composite films differ from those in pure PVB due to the strong

interaction between PVB and ZnO NPs [22, 23]. The hydroxyl groups of the PVB chains contribute to the changes in absorption intensity and irregular shifts.

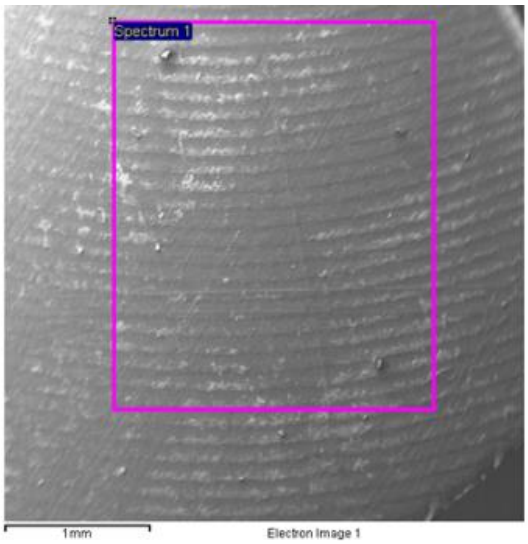

Element	Weight%	Atomic%
Carbon	69.52	75.55
Oxygen	29.79	24.30
Zinc	0.68	0.14
Total	99.99	99.99

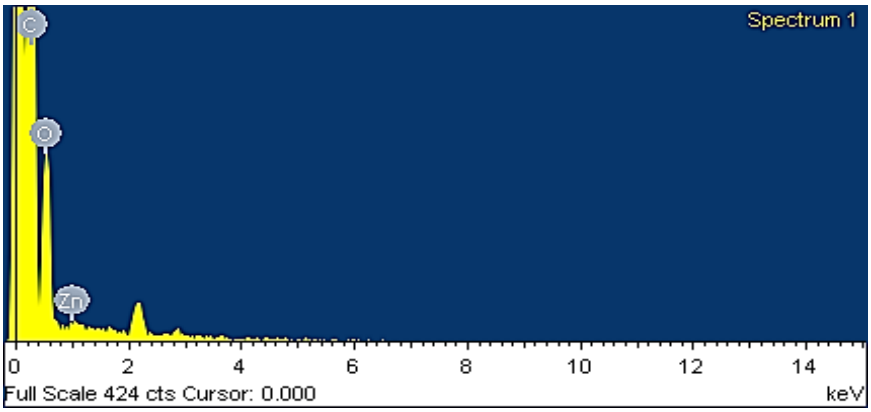

Figure 7. (b) EDS spectrum of 1.0 wt.% ZnO/PVB and elemental analysis.

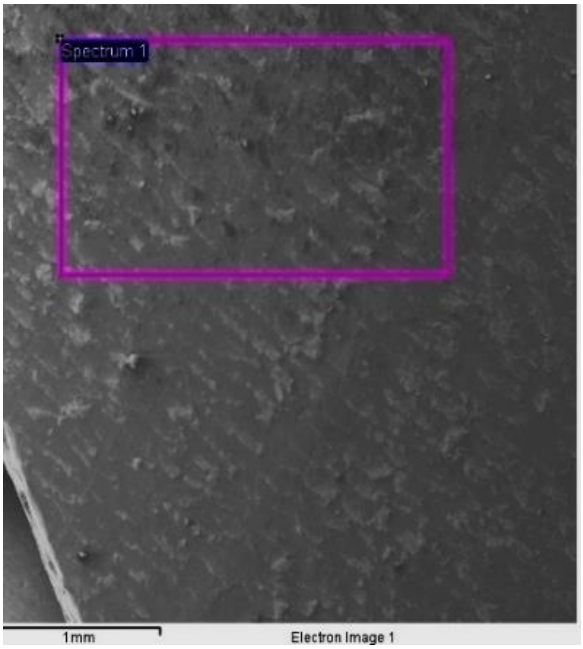

Element	Weight%	Atomic%
Carbon	71.60	77.87
Oxygen	26.68	21.78
Zinc	1.70	0.34
Total	99.99	99.99

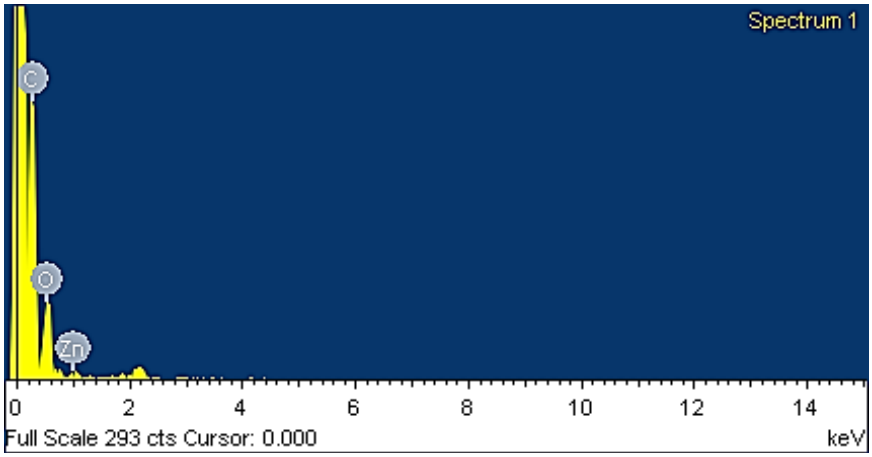

Figure 7. (c) EDS spectrum of 2.0 wt.% ZnO/PVB and elemental analysis.

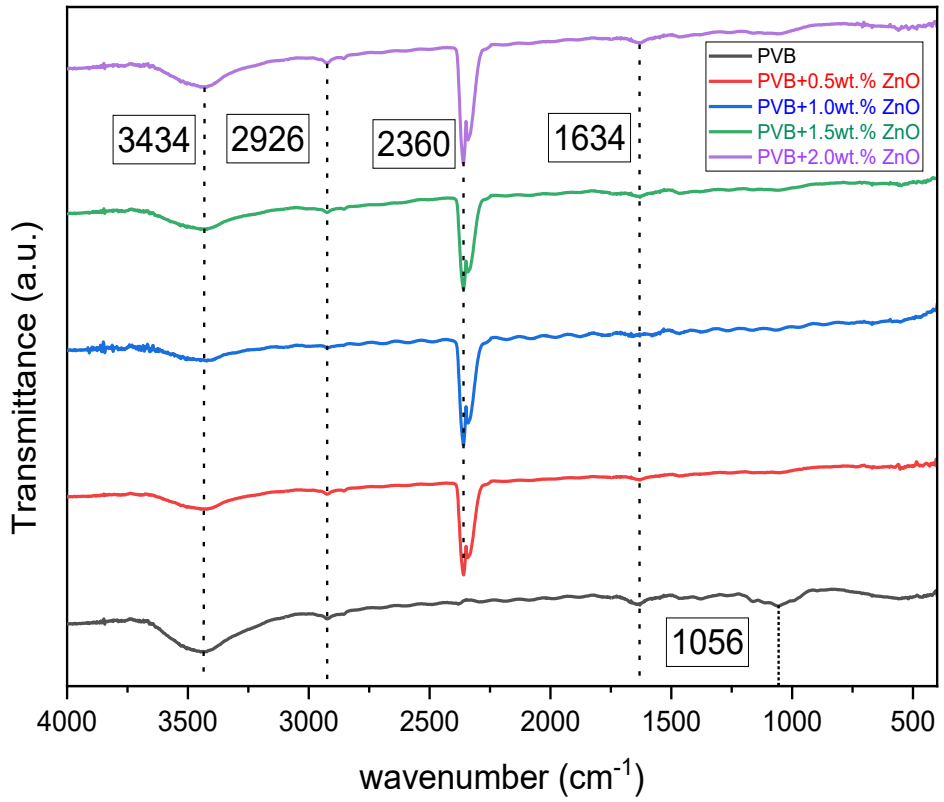

Figure 8. Representative FTIR signatures of pure PVB and ZnO/PVB nanocomposite films.

Table 2. FTIR peak assignments of pure PVB and ZnO/PVB composite films.

S.N.	Peak Position (cm^{-1})		Observation	Functional Group	Appearance	Comments
	Pure PVB	*Composite Films*				
1.	3342	3434	O–H Stretching	Hydroxyl	Strong/broad	Intermolecular bonded
2.	2923	2926	CH_2 Stretching	Alkane	Medium	Asymmetric stretching
3.	–	2360	H–O–H vibration	Water molecule	Strong	Crystallization
4.	1633	1634	C=O Stretching	Acetyl	Medium	Scissor bending vibrations
5.	1056	–	C–C Stretching	Butyral ring	Medium/broad	Asymmetric stretching

The change in the bending of CH_2 vibrations provides a chemical fingerprint for the interactions of ZnO with the PVB chains. Additionally, the frequency change of PVB acetyl C=O stretching offers further evidence of an interaction. The charge transfer process between the PVB main chains and the NPs may also contribute to the formation of new bonds. These insights support the dominant interaction between ZnO particles and the PVB acetyl group occurring at the inter/intramolecular level [24, 25]. These results confirm the successful formation of stable PVB composite films containing ZnO nanofiller with hydrogen bonding.

Optical Absorption

Figure 9 displays the absorption spectra of pure PVB and ZnO/PVB nanocomposite films and the data obtained at 25°C for analysis. Three absorption peaks at 215, 279, and 333 nm are identified in the spectra of pure PVB samples. These peaks correspond to the $–(CH=CH)_4–CO–$ groups on the polymer's backbone, π–π* transition, and n–π* transitions, respectively [26–28]. The peaks at 279 and 333 nm of pure PVB may be attributed to carbonyl functional groups [29]. A significant absorbance is observed between 220 and 250 nm, corresponding to the band gap of PVB and indicating the amorphous nature of the polymer [30]. The XRD analysis also revealed that the PVB polymer was amorphous.

The absorption edge of ZnO/PVB composite films was observed in the 250–340 nm region. In addition, a small absorbance peak is noted at ~350 nm at a higher concentration. This peak's energy gap is 3.37 eV, which confirms the presence of ZnO NPs in the composite films [6]. The redshift in the absorption edge of the nanocomposites indicated that a small amount of nanofiller could modify the optical band gap of PVB [31]. This absorption edge shift revealed hydrogen bonds between the –OH groups of the PVB polymer and the ZnO NPs. Figure 9 demonstrates that the optical absorption edge moved to longer wavelengths with increasing nanofiller concentration, as the absorption increment is connected to the charge-transfer transition [32]. Furthermore, when the samples were observed normally, the film's color changed from completely clear (pure PVB) to semitransparent (composite films). According to the above results, the nanocomposite films have absorbed radiation across a broad spectrum. Consequently, the synthesized films might be effective ultraviolet absorbers [30].

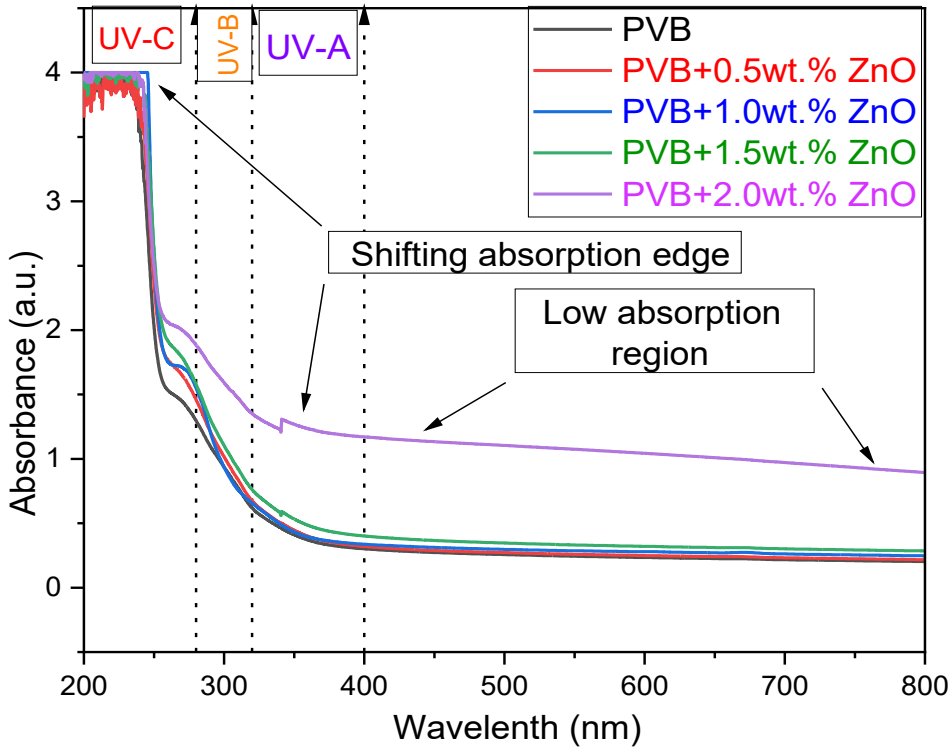

Figure 9. Absorbance as a function of wavelength for pure PVB and ZnO/PVB composite films.

Shielding of UV Radiation

The UV-visible spectra demonstrates that the PVB polymer absorbs energy between 200 and 280 nm, indicating that it can effectively block UV-C light. Pure PVB has a large bandgap of 4.5–5.0 eV, which corresponds to energy in the UV-C region. Observations showed that it could block up to 82% of UV light. Therefore, PVB films shield against UV rays and provide protection [31–35]. However, the UV-visible spectroscopy indicated that pure PVB film will completely block UV-C [36]. Furthermore, enhancing UV absorption in the polymer is necessary to protect against UV-A and UV-B. The UV protection of the PVB polymer can be further improved by dispersing nanofillers, which would lead to better UV shielding.

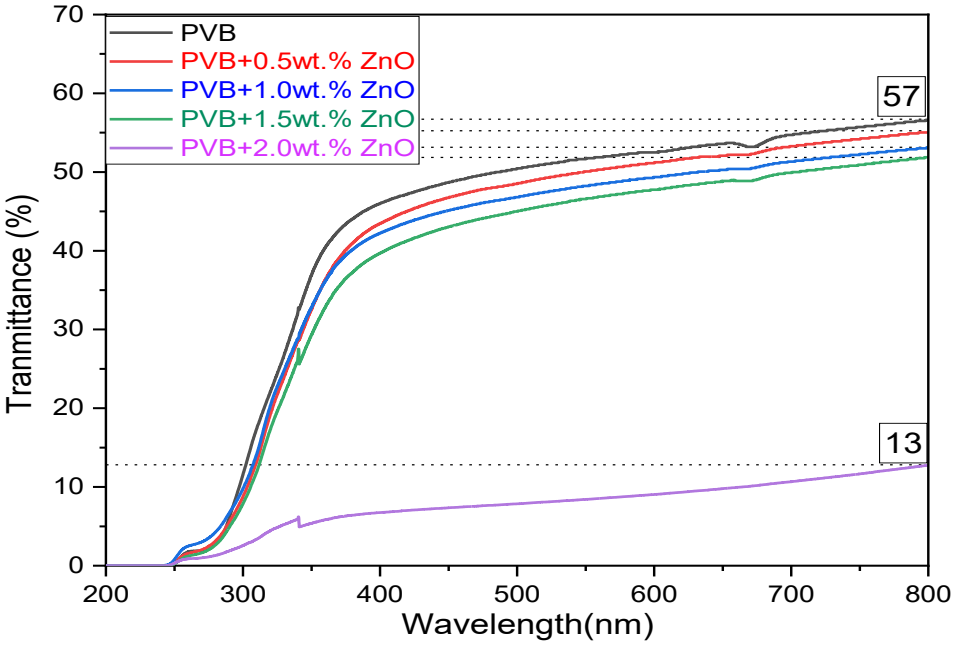

Figure 10. Transmittance as a function of wavelength for pure PVB and ZnO/PVB composite films.

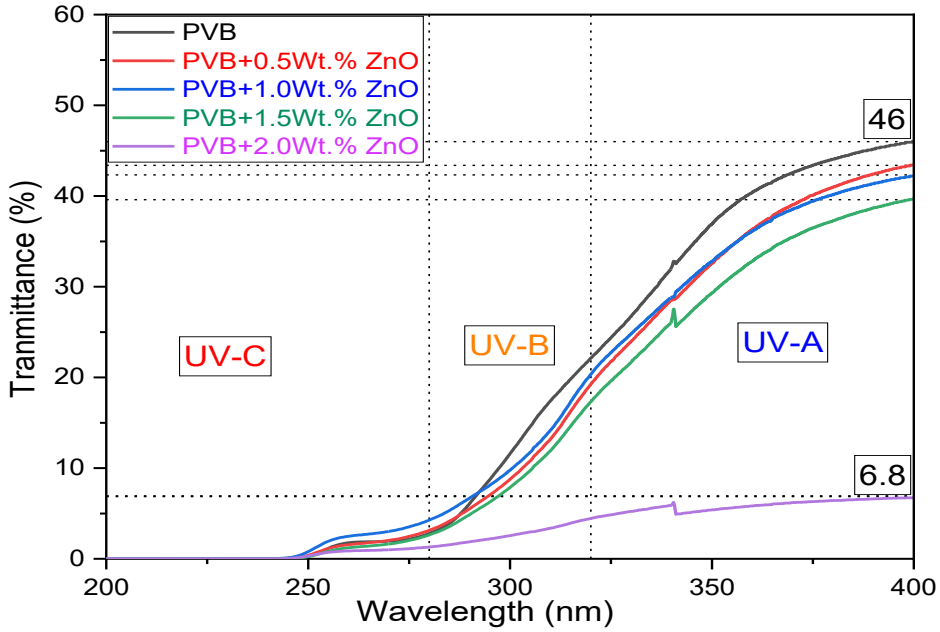

Figure 11. Transmittance as a function of wavelength for pure PVB and ZnO/PVB composite films in the UV region.

Figures 10 and 11 show that pure PVB film has very low (close to zero) transmittance up to 250 nm, completely blocking UV-C radiation. After 260 nm, UV transmission increases to 46% up to 400 nm. The percentage blocking of UV was calculated from the transmittance data using Equations 1, 2, and 3 in different regions.

The percentage blocking for UV-A (320–400 nm) was calculated by Eq. (1)

$$\text{UV-A blocking (\%)} = 100 - \frac{\int_{320}^{400} T(\lambda)d\lambda}{\int_{320}^{400} d\lambda} \text{ (\%)} \quad (1)$$

The percentage blocking for UV-B (280–320 nm) was calculated by Eq. (2)

$$\text{UV-B blocking (\%)} = 100 - \frac{\int_{280}^{320} T(\lambda)d\lambda}{\int_{280}^{320} d\lambda} \text{ (\%)} \quad (2)$$

The percentage blocking for UV-C (200–280 nm) was calculated by Eq. (3)

$$\text{UV-C blocking (\%)} = 100 - \frac{\int_{200}^{280} T(\lambda)d\lambda}{\int_{200}^{280} d\lambda} \text{ (\%)}. \quad (3)$$

In particular, the composite films containing 2.0 wt.% of ZnO in PVB provide up to 21.4% shielding while maintaining acceptable transparency. This improvement is quite impressive compared to pure PVB. The transmittance in the UV range (UV-A and UV-B) decreases from 46% to 6.8% when 2.0 wt.% of ZnO is dispersed, which affects the transparency in the visible range. This indicates a significant amount of UV blocking in the range from 260 nm to 400 nm with an increasing concentration of ZnO. The increase in UV blocking is primarily due to ZnO NPs. Conversely, the visible transmittance decreases with increasing ZnO wt.% due to scattering and agglomeration [34, 35].

Composites containing 0.5 wt.% reinforcement exhibit a 10% improvement in UV shielding compared to PVB. Adding 0.5 wt.% ZnO blocks UV wavelengths much more effectively than 2.0 wt.% [36]. Simultaneously, they are significantly more transparent in the visible range than pure PVB. Therefore, it is an excellent translucent composite film for everyday applications. Furthermore, PVB with 2.0 wt.% of ZnO is suitable for practical applications, displaying a well-defined visible light transmittance of 1.14 and a very high UV shielding of up to 96.98% (200–400 nm) compared to pure PVB. Each transmittance obtained was used to calculate the transparency value of the samples using Equation 4.

$$\text{Transparency value} = \log (T_{600}/d), \quad (4)$$

where T_{600} is the percentage transmittance (%) at 600 nm and d is the film thickness (in mm).

From the analysis, the overall transmittance decreased with increasing ZnO concentration, and a very low loss of visibility in polymer composite films was observed. This can also be seen in digital photographs of films. Table 3 shows detailed UV protection data from 200 to 400 nm, with three UV regions and their transparency. Strong UV-A and UV-B shielding was also observed for all ZnO/PVB composites compared to neat PVB films.

The loss of transparency in polymer-based composites can be attributed to several factors, including the molding of the polymer, the size of the reinforcement filler, particle aggregation, and light scattering by particles [37].

Another reason for the scattering could be NP aggregation due to its “high surface energy and surface-to-volume ratio.” Aggregates behave, like larger particles, blocking and scattering the light that passes

through them. The concentration of NPs also directly affects the transparency of the composites. It has been found that the size of agglomeration increases with the concentration of NPs. These ZnO aggregations are expected to result in strong scattering and a loss of transparency. The random dispersion of NPs in the matrix at high concentrations effectively blocks UV-A and UV-B radiation. This is due to the combined effects of larger particle size and particle agglomeration.

Table 3. UV-shielding parameters for the PVB and ZnO/PVB nanocomposite films.

S.N.	Sample	Percentage Blocking				Transparency
		UV	*UV-A*	*UV-B*	*UV-C*	
1.	PVB	82.20	61.90	87.45	99.00	2.93
2.	PVB+0.5wt.% ZnO	83.41	64.12	87.49	99.14	2.23
3.	PVB+1.0wt.% ZnO	83.62	61.81	89.53	99.19	2.21
4.	PVB+1.5wt.% ZnO	85.55	68.51	91.48	99.47	2.14
5.	PVB+2.0wt.% ZnO	96.98	94.10	97.25	99.62	1.43

Absorption Edge

Lambert Beer's relation (5) was utilized to determine the absorption coefficient (α) of the nanocomposite film with a thickness (t) [38].

$$\alpha = 2.303\left(\frac{A}{t}\right) \tag{5}$$

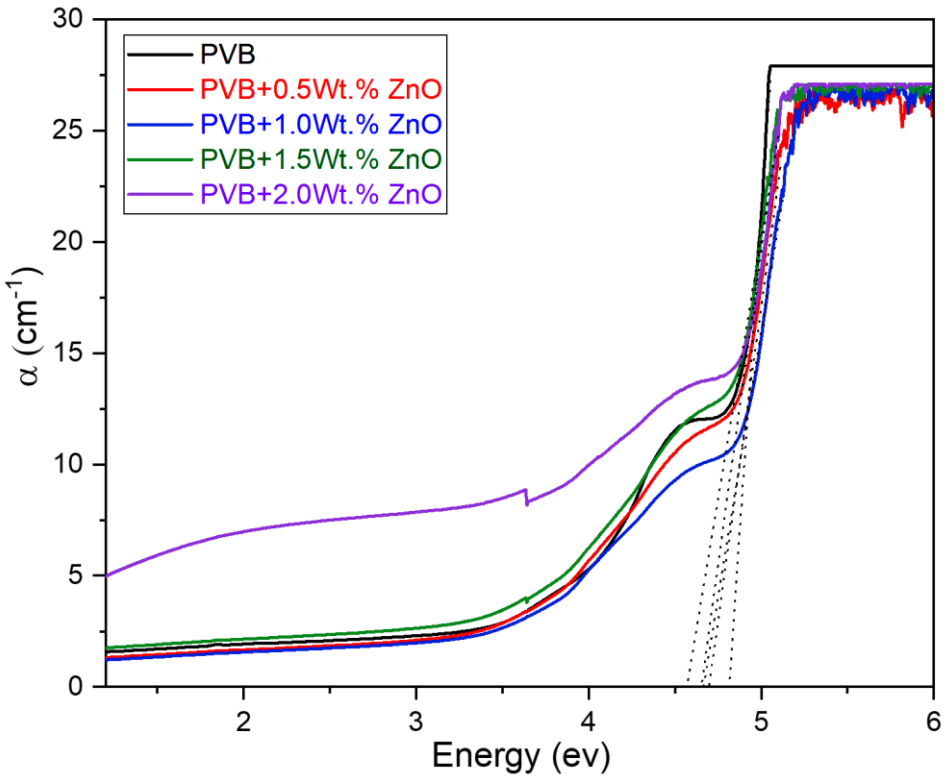

Figure 12. Absorption coefficient versus energy plots for pure PVB and ZnO/PVB composite films.

A graph was drawn to visualize the relationship between α and hυ. The absorption edge of the films was determined by extrapolating the linear region of the curves to the horizontal axis, as shown in Figure 12. The values of the absorption edge were calculated to be 4.84, 4.72, 4.65, 4.62, and 4.55 eV for PVB composite films dispersed with 0, 0.5, 1.0, 1.5, and 2.0 wt.% of ZnO, respectively. The absorption edge was lowered to 4.55 eV (whereas it is 4.84 eV for pure PVB) when 2.0 wt.% of ZnO

was dispersed in the PVB matrix [39], and the values are provided in Table 4. From the results, the absorption edge of the composite films decreases as the wt.% of ZnO NPs increases. This decrease in the absorption edge indicates an increase in the amorphous nature of the composite films.

Direct Bandgap and Indirect Bandgap Energies

We can determine the direct bandgap, indirect bandgap, and Urbach energy of amorphous and crystalline materials using UV-visible absorption spectra. Calculations were performed to evaluate the band gaps of the nanocomposite films near the absorption edge. Tauc's equation can assess the relationship between the absorption coefficient and the energy of incident photons [40] using Equation 6.

$$(\alpha h\upsilon) = k\,(h\upsilon - E_g)^{n}, \tag{6}$$

where k is the energy-independent constant, E_g is the optical bandgap energy, and n is the nature of the transition, it can take any of the following 2 values. (1) n = 1/2 for direct allowed bandgap transition and (2) n= 2 for indirect allowed bandgap transition.

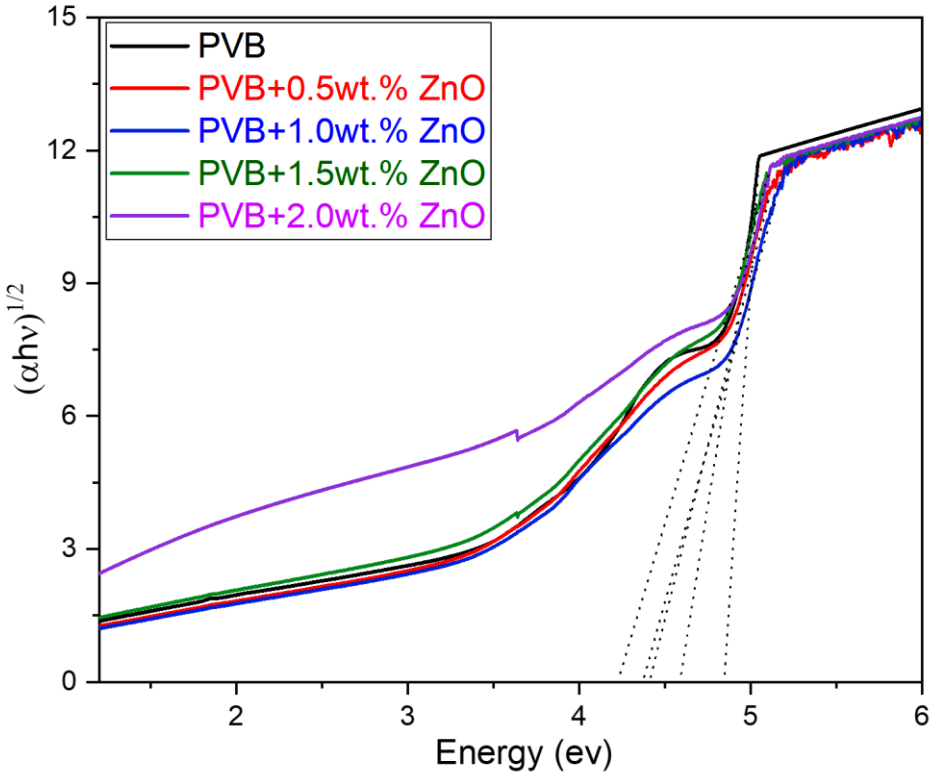

Figure 13. $(\alpha h\upsilon)^{1/2}$ versus $(h\upsilon)$ plots for pure PVB and ZnO/PVB composite films.

A plot of $(\alpha h\upsilon)^{1/2}$ against $h\upsilon$ was drawn to determine the direct band gap energy. The results of these calculations are shown in Figure 13. The indirect band gap energy was estimated by extrapolating the linear portion of the $(\alpha h\upsilon)^2$ versus $h\upsilon$ curve. From the observations, E_g reduced as the concentration of nanofiller increased. The results in Table 4 indicate that the direct band gap value dropped to 4.57 eV after adding 0.5 wt.% of ZnO to the PVB polymer, down from 4.62 eV for pure PVB. Previous research indicates that when a higher level of disorder is introduced into a non-crystalline inorganic material, the energy band gap shifts toward a lower energy level [40].

The indirect bandgap energy was obtained by extrapolating the linear part of the curve. Figure 14 illustrates the influence of ZnO content on the indirect bandgap of nanocomposite films. The results indicate that by dispersing 0.5 wt.% ZnO nanofiller, the indirect bandgap energy decreased from 4.90 eV for pure PVB to 4.88 eV. The changes in the bandgap values of nanocomposites may be attributed

to complex formation caused by the interaction of ZnO NPs with the polar (hydroxyl) groups of PVB [30, 31]. The interaction of ZnO with the hydroxyl groups of the PVB polymer resulted in aggregate formation, which affected the energy states of PVB [35]. Furthermore, incorporating ZnO into the polymer matrix creates additional localized defect states in the optical bandgap [40].

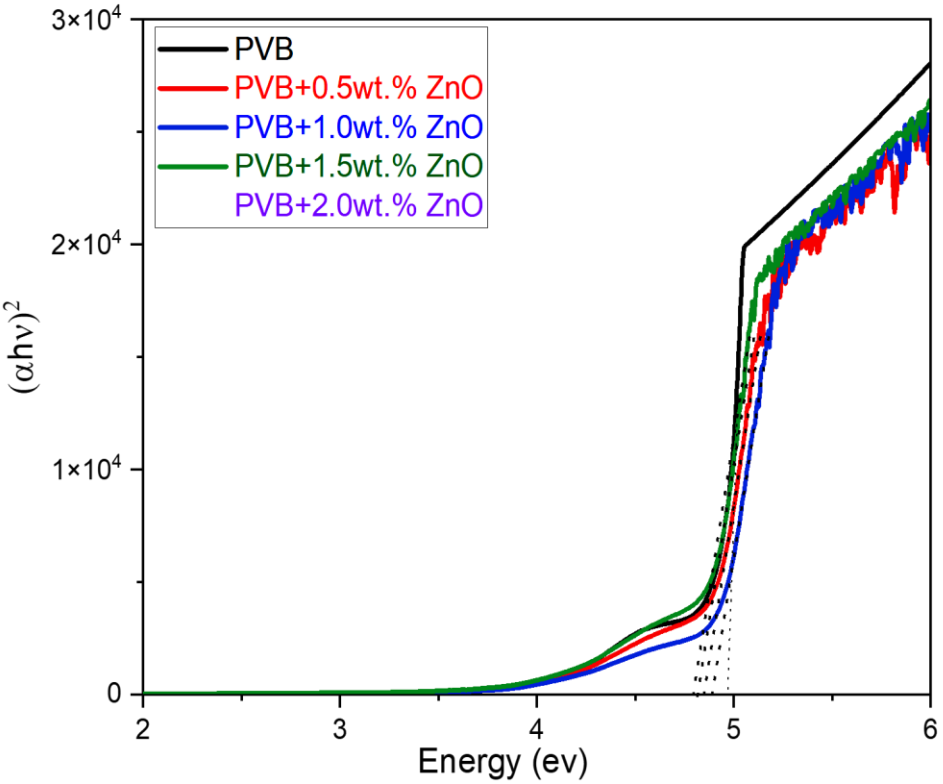

Figure 14. $(\alpha h\upsilon)^2$ versus $(h\upsilon)$ plots for pure PVB and ZnO/PVB composite films.

Table 4. Absorption edge, direct, indirect bandgap, and Urbach energy values of pure PVB and ZnO/PVB composite films.

S.N.	Composite	Absorption Edge (eV)	Direct Bandgap (eV)	Indirect Bandgap (eV)	Urbach Energy (eV)
1.	Pure PVB	4.84	4.62	4.90	0.73
2.	PVB + 0.5wt.% ZnO	4.72	4.57	4.88	0.76
3.	PVB + 1.0wt.% ZnO	4.65	4.42	4.87	0.79
4.	PVB + 1.5wt.% ZnO	4.62	4.36	4.84	0.83
5.	PVB + 2.0wt.% ZnO	4.55	4.22	4.81	1.48

Urbach Energy (E_u)

Urbach energy has been determined using Equation 7.

$$\ln(\alpha)=\ln(c)+ h\upsilon/E_u, \quad (7)$$

where C is a constant, the E_u was estimated by plotting $\ln(\alpha)$ against $h\upsilon$ and then calculating the slope of the linear portion of the graph, as shown in Figure 15. The graphs illustrate the influence of the amount of nanofiller on the E_u of the samples. The E_u values increased with the amount of nanofiller. The E_u value changed to 0.76 eV after being dispersed with ZnO content of 0.5 wt.%, from 0.73 eV for pure PVB. This suggests that lattice thermal vibrations are enhanced with the content of ZnO.

The dispersion of the ZnO nanofiller causes shifts in the bandgap energy and band tail, resulting in modifications to the energy states of PVB. Due to these changes, localized states are generated in the forbidden bandgap of the polymer matrix, which could affect the Fermi level. These states are accountable for determining the optoelectrical aspects of the nanocomposites, in addition to serving as recombination and trapping centers. Therefore, by increasing the low-energy transitions, the bandgap is reduced, the band tail width is expanded, and the optoelectrical conductivity of the composite films is improved [35, 36].

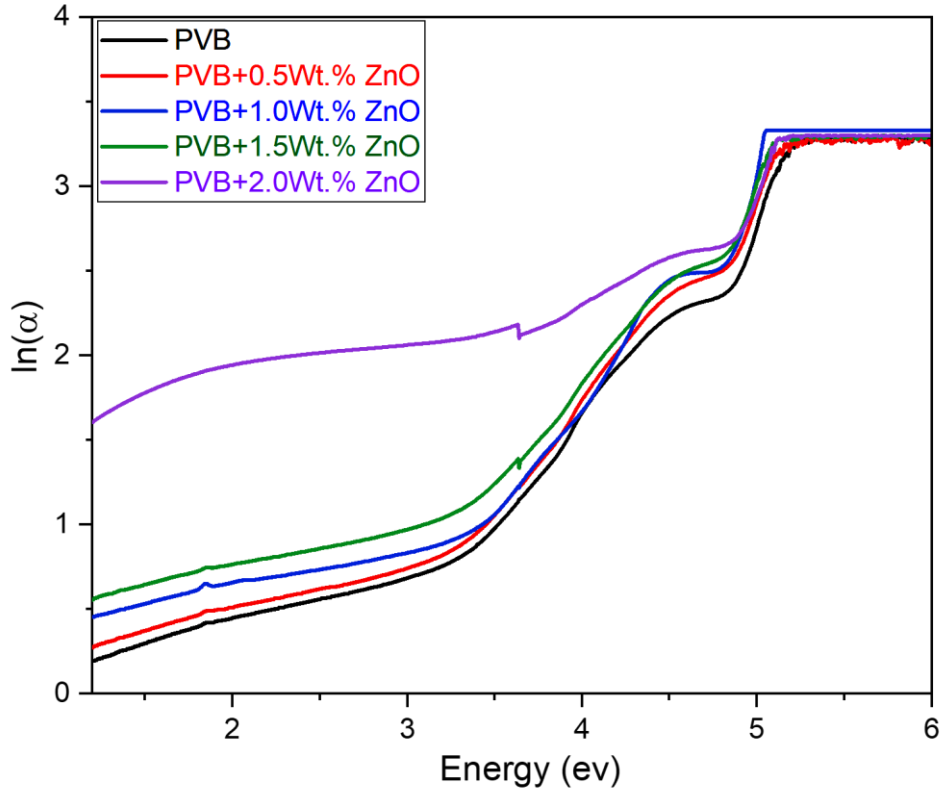

Figure 15. ln(α) versus hν plot for Urbach energy calculations of pure PVB and ZnO/PVB nanocomposite films.

CONCLUSIONS

This study aims to prepare PVB nanocomposites with ZnO nanofiller and investigate the influence of the loading percentage of ZnO. The dispersion of ZnO NPs within the PVB polymer is responsible for the change in intensity of the crystalline peaks. This occurs due to hydrogen bonding between the OH groups of PVB and the ZnO NPs, leading to an increase in the intermolecular distances of the PVB chains. The morphology of the composites reveals a typical nanocluster structure composed of numerous ZnO nanospheres. All the ZnO/PVB nanocomposites exhibited rough surfaces, differing considerably from the smooth surface of pure PVB, indicating that ZnO had been effectively dispersed in the PVB polymer. The minor peaks in the FTIR spectra between 518 and 560 cm^{-1} in the composite films reveal the presence of ZnO NPs. The irregular shifts result from the hydroxyl groups in the PVB chain, contributing to the formation of stable complex chemical composites interrelated with NPs. The change in the bending of CH_2 vibrations provides a chemical fingerprint for the interactions of ZnO with the PVB chains.

The optical absorption increases with the wt.% of ZnO NPs because the absorption increment is linked to the charge-transfer transition. The absorbance spectrum of the nanocomposites suggested that increasing the amount of ZnO wt.% in composite films could enhance the UV-shielding properties of

the PVB. From the observations, the prepared composite films have high UV absorption and acceptable transparency for visible light. So these composite films have been used as effective UV-stabilized materials for various outdoor applications with high sunlight loads.

REFERENCES

1. Barzinjy A. Structure, synthesis and applications of ZnO nanoparticles: A review. Jord J Phys. 2020;13(2):123–35.
2. Vaseem M, Umar A, Hahn YB. ZnO nanoparticles: growth, properties, and applications. Metal Ox Nano Appl. 2010;5(1):10–20.
3. Wahab HA, Salama AA, El Saeid AA, Willander M, Nur O, Battisha IK. Zinc oxide nano-rods based glucose biosensor devices fabrication. Res Phys. 2018;9:809–14.
4. Lakshmipriya T, Gopinath SC. Introduction to nanoparticles and analytical devices. In: Nanoparticles in analytical and medical devices. Elsevier; 2021. pp. 1–29.
5. Baxter JB, Aydil ES. Nanowire-based dye-sensitized solar cells. Appl Phys Lett. 2005;86(5):053114.
6. Huang MH, Mao S, Feick H, Yan H, Wu Y, Kind H, et al. Room-temperature ultraviolet nanowire nanolasers. Science. 2001;292(5523):1897–9.
7. Song J, Zhou J, Wang ZL. Piezoelectric and semiconducting coupled power generating process of a single ZnO belt/wire. A technology for harvesting electricity from the environment. Nano Lett. 2006;6(8):1656–62.
8. Wang ZL. Functional oxide nanobelts: Materials, properties and potential applications in nanosystems and biotechnology. Ann Rev Phys Chem. 2004;55(1):159–96.
9. Sawai J, Kawada E, Kanou F, Igarashi H, Hashimoto A, Kokugan T, et al. Detection of active oxygen generated from ceramic powders having antibacterial activity. J Chem Eng Japan. 1996;29(4):627–33.
10. Minne SC, Manalis SR, Quate CF. Parallel atomic force microscopy using cantilevers with integrated piezoresistive sensors and integrated piezoelectric actuators. App Phys Lett. 1995;67(26):3918–20.
11. Que M, Lin C, Sun J, Chen L, Sun X, Sun Y. Progress in ZnO nanosensors. Sensors. 2021;21(16):5502.
12. Kołodziejczak-Radzimska A, Jesionowski T. Zinc oxide—from synthesis to application: A review. Materials. 2014;7(4):2833–81.
13. Li X, He G, Xiao G, Liu H, Wang M. Synthesis and morphology control of ZnO nanostructures in microemulsions. J Coll Interf Sci. 2009;333(2):465–73.
14. Selvi J, Parthasarathy V, Mahalakshmi S, Anbarasan R, Daramola MO, Senthil Kumar P. Optical, electrical, mechanical, and thermal properties and non-isothermal decomposition behavior of poly (vinyl alcohol)–ZnO nanocomposites. Iran Polym J. 2020;29:411–22.
15. Kumar NB R, Crasta V, Praveen BM, Kumar M. Studies on structural, optical and mechanical properties of MWCNTs and ZnO nanoparticles doped PVA nanocomposites. Nanotech Rev. 2015;4(5):457–67.
16. Vera Garcia PF, Guerrero Dimas LA, Cedillo Portillo JJ, Martínez Anguiano OA, Sáenz Galindo A, Narro Cespedes RI, et al. PVA blends and nanocomposites, properties and applications: A review. Green-Based Nanocomp Mat App. 2023;191–206.
17. Krishnamoorti R. Strategies for dispersing nanoparticles in polymers. MRS Bull. 2007;32(4):341–7.
18. Wang H, Qiu X, Liu W, Fu F, Yang D. A novel lignin/ZnO hybrid nanocomposite with excellent UV-absorption ability and its application in transparent polyurethane coating. Industr Eng Chem Res. 2017;56(39):11133–41.
19. Terziyan TV, Safronov AP, Beketov IV, Medvedev AI, Armas SF, Kurlyandskaya GV. Adhesive and magnetic properties of polyvinyl butyral composites with embedded metallic nanoparticles. Sensors. 2021;21(24):8311.
20. Bai Y, Zhang J, Wen D, Gong P, Chen X. A poly (vinyl butyral)/graphene oxide composite with NIR light-induced shape memory effect and solid-state plasticity. Comp Sci Tech. 2019;170:101–8.

21. Muhammad W, Ullah N, Haroon M, Abbasi BH. Optical, morphological and biological analysis of zinc oxide nanoparticles (ZnO NPs) using *Papaver somniferum* L. RSC Adv. 2019;9(51):29541–8.
22. Deorukhkar OA, Radhakrishnan S, Munde YS, Kulkarni MB. Polymer nanocomposites: Polymer composites: Design, manufacturing, and applications. Polym Based Comp. 2021:73–95.
23. Pizzanelli S, Forte C, Bronco S, Guazzini T, Serraglini C, Calucci L. PVB/ATO nanocomposites for glass coating applications: Effects of nanoparticles on the PVB matrix. Coatings. 2019;9(4):247.
24. Akman E, Sonmezoglu S, Yigit E, Eskizeybek V, Avci A. Hybrid nanoparticles embedded polyvinyl butyral nanocomposites for improved mechanical, thermal and microwave absorption performance. J Comp Mat. 2021;55(29):4431–44.
25. Goutam SP, Yadav AK, Das AJ. Coriander extract mediated green synthesis of zinc oxide nanoparticles and their structural, optical and antibacterial properties. J Nanosci Tech. 2017:249–52.
26. Aslam M, Kalyar MA, Raza ZA. Fabrication of nano-CuO-loaded PVA composite films with enhanced optomechanical properties. Polym Bull. 2021;78:1551–71.
27. Qiao Y, Duan L. Curcumin-loaded polyvinyl butyral film with antibacterial activity. e-Polymers. 2020;20(1):673–81.
28. Kumar NB R, Crasta V, Praveen BM, Kumar M. Studies on structural, optical and mechanical properties of MWCNTs and ZnO nanoparticles doped PVA nanocomposites. Nanotech Rev. 2015;4(5):457–67.
29. Olson E, Li Y, Lin FY, Miller A, Liu F, Tsyrenova A, et al. Thin biobased transparent UV-blocking coating enabled by nanoparticle self-assembly. ACS Appl MatI Interf. 2019;11(27):24552–9.
30. Wang Y, Su J, Li T, Ma P, Bai H, Xie Y, et al. A novel UV-shielding and transparent polymer film: When bioinspired dopamine–melanin hollow nanoparticles join polymers. ACS Appl Mat Interf. 2017;9(41):36281–9.
31. Espejo C, Arribas A, Monzo F, Diez PP. Nanocomposite films with enhanced radiometric properties for greenhouse covering applications. J Plast Film Sheet. 2012;28(4):336–50.
32. Fu Y, Huang Y, Meng W, Wang Z, Bando Y, Golberg D, et al. Highly ductile UV-shielding polymer composites with boron nitride nanospheres as fillers. Nanotechnology. 2015;26(11):115702.
33. Reddy R, Narsimlu N. Simultaneous enhancements of UV-shielding properties and photostability of polyvinyl butyral by incorporation of MWCNTs. Optic Mat. 2024;154:115687.
34. Fu X, Yu Y, Feng J, Ng KM. Fabrication of transparent and photoluminescent poly (vinyl butyral)/carbon dots nanocomposite thin film. Mat Res Exp. 2015;2(2):026403.
35. Emir P, Kuru D. Boron nitride quantum dots/polyvinyl butyral nanocomposite films for the enhanced photoluminescence and UV shielding properties. J Appl Polym Sci. 2024;141(13):e55171.
36. Fu Y, Huang Y, Meng W, Wang Z, Bando Y, Golberg D, et al. Highly ductile UV-shielding polymer composites with boron nitride nanospheres as fillers. Nanotechnology. 2015;26(11):115702.
37. Sharma S, Vyas R, Srivastava S, Vijay YK. Preparation and characterization of transparent ZnO/polymethyl methacrylate nanocomposites. In: AIP Conference Proceedings. American Institute of Physics. 2011 Oct 20;1391(1):627–629.
38. Muhmood AA, Zgair IA, Hussein MA, Mahdi LH, Jabbar BS, Alkhayatt AH. Preparation and optical characterizations of PVA: Ag Nano composite. In: Journal of Physics: Conference Series. IOP Publishing. 2021 May 1;1879(3):032083.
39. Mohammed MI, Khafagy RM, Hussien MS, Sakr GB, Ibrahim MA, Yahia IS, et al. Enhancing the structural, optical, electrical, properties and photocatalytic applications of ZnO/PMMA nanocomposite membranes: Towards multifunctional membranes. J Mat Sci: Mat Electron. 2021;1–26.
40. Indolia AP, Gaur MS. Optical properties of solution grown PVDF-ZnO nanocomposite thin films. J Polym Res. 2013;20:1–8.

